Proceedings of the World Congress on Engineering 2008 Vol I
WCE 2008, July 2 - 4, 2008, London, U.K.

A GA-based Approach for Parameter Estimation in DT-MRI Tracking Algorithms

L.M. San-José-Revuelta, M. Martín-Fernández and C. Alberola-López *

Abstract— **This paper expands upon previous work of the authors in the field of fiber tracking in diffusion tensor (DT) fields acquired via magnetic resonance (MR) imaging. Specifically, we now focus on tuning-up a previously developed probabilistic tracking algorithm by making use of a novel genetic algorithm which helps to optimize most of the adjustable parameters of the tracking algorithm. Since the adjustment of these parameters constitutes a hard NP-complete problem, traditionally, this task has been heuristically approached. A year ago, we presented in the WCE'07 a multilayer neural network that was successfully applied to this issue. Its robustness and complexity were studied with more detail in the extended version recently published in the IAENG journal on Computer Science. Sine complexity constituted its main drawback, in this paper we explore the possibility of using a computationally simpler method based on a micro-genetic algorithm. This strategy is shown to outperform the NN-based scheme, leading to more robust, efficient and human independent tracking schemes.**

Keywords: diffusion tensor magnetic resonance imaging, fiber tracking, genetic algorithm

1 Introduction

The Diffusion Tensor Magnetic Resonance Imaging (DT-MRI) technique measures the diffusion of hydrogen atoms within water molecules in 3D space. Since in cerebral white matter most random motion of water molecules are restricted by axonal membranes and myelin sheets, diffusion anisotropy allows depiction of directional anisotropy within neural fiber structures [1, 2]. The DT-MRI technique has raised great interest in the neuro-science community for a better understanding of the fiber tract anatomy of the human brain. Among the many applications that arise from tractography we find: brain surgery (knowing the extension of the fiber bundles could minimize the functional damage to the patient), white matter visualization using fiber traces (for a better understanding of brain anatomy) and inference of connectivity between different parts of the brain (useful for functional and morphological research of the brain).

*ETSI Telecomunicación, University of Valladolid, 47010 Valladolid, Spain. Tel: +34-983-423660, Fax: +34-983-423667. Email: lsanjose@tel.uva.es.

Most of DT-MRI visualization techniques focuses on the integration of sample points along fiber trajectories [7], using only the principal eigenvector of the diffusion ellipsoid as an estimate of the predominant direction of water diffusion [2]. However, these methods may depict some fiber tracts which do not exist in reality or miss to visualize important connectivity features, e.g. crossing or branching structures. In order to avoid misinterpretations, the viewer must be provided with some information on the uncertainty of every depicted fiber and of its presence in a certain location. In [9] we proposed an estimation algorithm that takes into account the whole information provided by the diffusion matrix, i.e., it does not only consider the principal eigenvector direction but the complete 3D information about the certainty of continuing the path through every possible future direction. An improved version of this algorithm was presented last year in WCE'07 [10]. This article included two main aspects: (i) a procedure that on-line adapts the number of *offspring paths* emerging from the actual voxel, to the degree of anisotropy observed in its proximity (this strategy was proved to enhance the estimation robustness in areas where multiple fibers cross while keeping complexity to a moderate level), and (ii) an initial version of a neural network (NN) for adjusting the parameters of the algorithm in a user-directed training stage. Subsequent work [11] studied with more detailed the architecture of the neural network and numerically evaluated its tracking capability, robustness and computational load when used with both synthetic and real DT-MR images. This work showed that in many cases, such as real images with low SNR, a huge computational load was required.

In this paper we propose to use an evolutionary computation-based approach for tuning-up the parameters of the tracking algorithm instead of using the neural network. The main aim is to adjust the parameters with a less complex procedure and to obtain a robust and efficient tracking algorithm. The required human intervention time should also be reduced. Specifically, we propose a genetic algorithm for this optimization task. Numerical results will prove that this approach leads to similar and even better convergence results while offering much lower computational requirements.

2 Brief Tracking Algorithm Description

Since our main purpose is the development of an algorithm to adjust the parameters of a tracking algorithm, it is necessary to outline the head expressions of this algorithm[1]. Thus, this section presents a brief summary of the method. The algorithm uses probabilistic criteria and iterates over several points in the analyzed volume (the points given by the highest probabilities in the previous iteration). The process starts in a user-selected seed voxel, V_0.

At every iteration, the method evaluates a set of parameters related to the central voxel of a cubic structure similar to that shown in Figure 1, left. The central point, V_c, (No. 14 in the figure) represents the last point of the tract being analyzed. In the first iteration, $V_c = V_0$.

2.1 Basic concepts

First, a measure P_i, $i \in \{valid\ points\}$, is evaluated based on the probability of going from voxel V_c to voxel V_i. This probability takes into account the eigenvalues and eigenvectors available at point V_c from the DT-MR image diffusion matrix. In order to calculate this probability, the information shown in Fig. 1, right, is used.

The table shows, for every voxel shown in Fig. 1, left, the changes that must occur in indices (m, n, p), when a tract goes from voxel V_c to voxel V_i. For instance: when going from point No. 14 to point No. 17, coordinates m and n increase by 1, and p remains the same. This is represented in the table with "$\pi_m\pi_n\pi_p = (+ + 0)$". With this information, the probability of each possible destination V_i can be calculated taking into account the projection of each of the eigenvectors to each of the directions defined in the triplet $\pi_m\pi_n\pi_p$. Besides, each projection is weighted by the corresponding eigenvalue λ. Thus, in the previous example, P_i should be calculated as $P_i = V_{1y}\lambda_1 + V_{2y}\lambda_2 + V_{3y}\lambda_3 + V_{1z}\lambda_1 + V_{2z}\lambda_2 + V_{3z}\lambda_3$, where $V_{j\alpha}$ represents the α-component of eigenvector j, $1 \leq j \leq 3$, $\alpha \in \{x, y, z\}$.

The axes reference criterion for the (x, y, z) vector components is also shown in Fig. 1. Note that, for this calculus, the sign "$-$" in the triplet is equivalent to sign "$+$". In order to properly calculate P_i, it must be weighed by 0.33 if there are no zeros in triplet i, and by 0.5 if there is one zero.

2.2 Anisotropy and local probability

The following anisotropy index is used in the algorithm:

$$\text{fa} = \sqrt{\frac{(\lambda_1 - \lambda_2)^2 + (\lambda_2 - \lambda_3)^2 + (\lambda_1 - \lambda_3)^2}{2(\lambda_1^2 + \lambda_2^2 + \lambda_3^2)}}, \qquad (1)$$

[1]For the sake of brevity, we the reader interested in a detailed development of this tracking algorithm can see the corresponding sections in [9].

where $\lambda_1 \geq \lambda_2 \geq \lambda_3$. When both $\text{fa}(V_c)$ and $\text{fa}(V_i)$ do not exceed a certain threshold, then point V_i is eliminated as a possible destination point.

Taking into account both P_i and the anisotropy given by Eq. (1), the local probability of voxel i is defined as

$$P_i' = a \cdot \mu_1 \cdot fa(V_i) + (1 - a) \cdot \mu_2 \cdot P_i, \qquad 0 < a < 1 \quad (2)$$

where parameter a allows the user to give a higher relative weight to either the anisotropy or the local probability, and μ_1 and μ_2 are scaling factors (normally, 1 and 1000, respectively). The set of values P_i' is properly normalized so that they can be interpreted as probabilities.

2.3 Eigenvectors and direction considerations

Besides these considerations, the final probability of voxel i makes also use of the so-called *smoothness parameters* (described in [5]) which judge the coherence of fiber directions among the trajectories passing through voxel V_c. The mathematical expressions of these four parameters, $\{sp_i\}_{i=1}^4$, as well as their geometrical meaning, is explained in [11]. They measure the angles between the directions that join successive path points, as well as the angles between these directions and the eigenvectors associated to the largest eigenvalues found in those voxels. sp_2, sp_3 and sp_4 are used to maintain the local directional coherence of the estimated tract and avoid the trajectory to follow unlikely pathways [5]. The threshold for sp_1 is set such that the tracking direction could be moved forward consistently and smoothly, preventing the computed path from sharp transitions.

Next, the following parameter is calculated for every valid point whose smoothness parameters satisfy the four corresponding threshold conditions,

$$P_i'' = b(\xi_1 sp_1 + \xi_2 sp_2 + \xi_3 sp_3 + \xi_4 sp_4) + (1 - b)P_i' \quad (3)$$

where, ξ_1, ξ_2, ξ_3 and ξ_4 are the corresponding weights of the smoothness parameters (normally, 0.25), and b stands for a weighting factor.

2.4 Path probabilities

Probabilities P_i'' can be recursively accumulated, yielding the probability of the path generated by the successive values of V_c,

$$P_p(k) = P_i''' \cdot P_p(k - 1) \qquad (4)$$

with k being the iteration number, and $P_i''' = P_i'' / \sum_i P_i''$.

At the end of the visualization stage, every estimated path is plotted with a color that depends on its probability P_p.

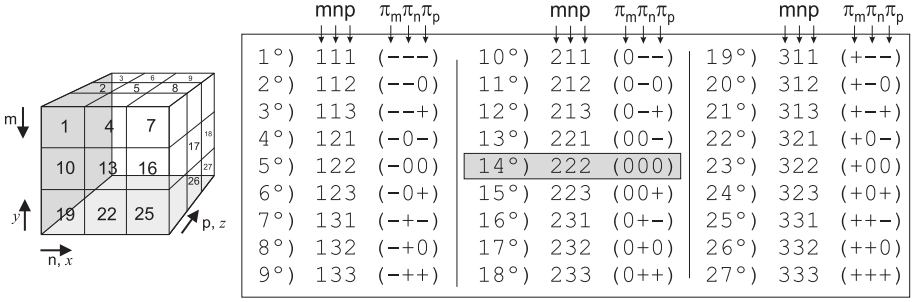

Figure 1: Modifications of indices (m, n, p) when moving from V_c to the neighboring voxel V_i, $1 \leq i \leq 27$, $i \neq 14$.

2.5 Final criterion and pool of "future seeds"

A pool of voxels is formed by selecting, at the end of each iteration, the s best voxels according to Eq. (3). The first voxel of the pool becomes the central voxel V_c at next iteration, expanding, this way, the current pathway.

As proposed in [11], the value of s is adjusted depending on the degree of anisotropy found in current voxel V_c and its surroundings. When this anisotropy is high, it means that a high directivity exists in that zone, and the probability that V_c belongs to a region where fibers cross is really low. Consequently, s takes a small value (1, 2 or 3). On the other hand, if V_c is found to be situated in a region of high anisotropy, the probabilities of having fibers crossing or branching is higher. In this case, it is interesting to explore various paths starting in V_c. This can be achieved by setting parameter s to a higher value.

2.6 Parameters to be estimated

In this paper we propose to use an genetic algorithm for adjusting the parameters of the algorithm $(a, b, \mu_1, \mu_2, \xi_1, \xi_2, \xi_3, \xi_4)$, instead of using the complex and time consuming NN proposed in [10, 11]. This adjustment is useful when the algorithm is applied to a different part of the brain (fiber bundles) or even to the same portion but having been scanned with under different conditions. In these cases, the volume of interest will have a different smoothness and anisotropy characterization.

3 Proposed GA for Parameter Estimation

Genetic algorithms (GAs) represent a set of potential solutions (*population*) with a predetermined encoding rule. At every iteration, each potential solution (*chromosome*) is associated to a figure of merit, or *fitness* value, in accordance to its proximity to the optimal solution. Considering the tracking problem described in Section 2, the goal is to estimate the set of algorithm's parameters and thresholds $\Omega = (a, b, \mu_1, \mu_2, \xi_1, \xi_2, \xi_3, \xi_4)$.

3.1 Estimation procedure

When this strategy is used, the user is requested to manually draw a sample fiber path as well as to compare this fiber path to those estimated by the GA during its first stages. Specifically, the steps for the estimation of the parameters are: (i) the user manually draws a sample fiber path, $\mathbf{r}_u$, (ii) the GA starts with a randomly generated population of $n_p = 10$ individuals $\{\mathbf{u}_i\}_{i=1}^{n_p}$, each of them being a possible binary representation of parameters Ω, (iii) the tracking algorithm of Section 2 is applied n_p times, each of them with the set of parameters represented by each GA's individual. This way, n_p different paths $\mathbf{r}_i$ are obtained, (iv) every path $\mathbf{r}_i$ is compared with $\mathbf{r}_u$ and given a fitness value λ_i, (v) iterate the GA during $n_g = 25$ generations and then go to step (ii).

Every time that the fiber paths are obtained at step (ii) the user must compare them to his sample $\mathbf{r}_u$ and, in case he finds that a tract $\mathbf{r}_j$, $1 \leq j \leq n_p$, is better than his first estimation $\mathbf{r}_u$, then $\mathbf{r}_j$ becomes the new reference path $\mathbf{r}_u$. At the end, solution Ω is obtained from the encoding of the fittest individual.

Though this scheme seems initially complicated, experiments show that a few iterations lead to sets Ω that allow to obtain good results when used in the tracking algorithm. The user will not have to assign too many fitness values or to perform many comparisons. The extremely reduced size of the population and the low number of generation per GA execution, derive in moderately short training periods.

3.2 GA description

The initial set of potential solutions, $\mathcal{P}[0]$ (population at $k = 0$), is randomly generated[2]. Let us denote $\mathcal{P}[k] = \{\mathbf{u}_i\}_{i=1}^{n_p}$ to the population at iteration k. As previously mentioned, the population size n_p has been fixed to a low value exploiting, this way, the properties of the so called *micro genetic algorithms* (μ-GA).

[2]In our specific application, the user drawn tract could be included in the initial population.

3.2.1 Genetic operators

In order to perform step (v) in subsection 3.1, individuals are modified by making use of the *genetic operators*, mainly *mutation* and *crossover*, to a subset of individuals selected using the *roulette wheel* selection scheme [6].

The mutation operator modifies specific individuals with probability p_m, changing the value of some concrete positions in the encoding of $\mathbf{u}_i$. Both the specific positions and the new values are randomly generated, and mutation is effectively performed with probability p_m. Notice that this genetic operator promotes the exploration of different areas of the solutions space.

On the other hand, the crossover operator requires two operands (*parents*) to produce two new individuals (*offspring*). These new individuals are created when merging parents by crossing them at specific internal points. This operation is performed with probability p_c. Since parents are selected from those individuals having a higher fitness, the small variations introduced within these individuals are intended to also generate high fit individuals.

3.2.2 Elitism and entropy dependent operators

The proposed GA also implements an elitism strategy: the best individual in the population is preserved and directly introduced in the new population. Nevertheless, a duplicate of it can also be used as input for the genetic operators.

Following the ideas described in [8], the crossover and mutation probabilities depend on the Shannon entropy of the population (excluding the elite) fitness, which is calculated as

$$\mathcal{H}(\mathcal{P}[k]) = -\sum_{i=1}^{n_p} \lambda_i^*(k) \log \lambda_i^*(k) \qquad (5)$$

with $\lambda_i^*(k)$ being the normalized fitness of individual $\mathbf{u}_i$, i.e., $\lambda_i^*(k) = \lambda_i(k) / \sum_{i=1}^{n_p} \lambda_i(k)$. When all the fitness values are very similar, with small dispersion, $\mathcal{H}(\mathcal{P}[k])$ becomes high and p_c is decreased–it is not worthwhile wasting time merging very similar individuals. This way, exploration is boosted, while, conversely, exploitation decreases. On the other hand, when this entropy is small, there exists a high diversity within the population, a fact that can be exploited in order to increase the horizontal sense of search. Following a similar reasoning, the probability of mutation is increased when the entropy is high, so as to augment the diversity of the population and escape from local suboptimal solutions (exploitation decreases, exploration becomes higher). Therefore, we have that probabilities p_m and p_c are directly/inversely proportional to the population fitness entropy, respectively.

As a consequence of these entropy dependent genetic operators, the resulting complexity of the GA is notably decreased since crossover is applied with a very low probability (and only on individuals not belonging to the elite), and the diversity control allows the algorithm to work properly with a much smaller population size [8].

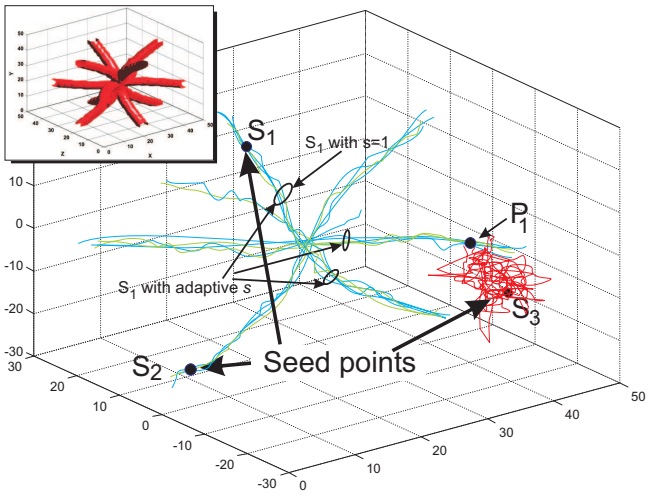

Figure 2: Tracking results for the "star" synthetic DT-MR image. Black: seed points. Blue: fiber paths obtained using adjustment with NN, Green: paths using estimation with the proposed AG. Red: extrinsic voxels. Initial seeds $V_0 = \{S_1, S_2, S_3\}$. Top left: original synthetic image.

4 Numerical Results

In order to evaluate the proposed algorithm (parameter tuning + tracking), both synthetic and real DT-MR images have been used. For the sake of comparison, we have used the same test images as in [11].

4.1 Synthetic images

Figure 6 in [11] shows four different synthetic DT-MRI data defined in a $50 \times 50 \times 50$ grid (we will refer to them as "cross", "earth", "log" and "star" as in previous work). To make the simulated field more realistic, Rician noise [4] was added in the diffusion weighted images which were calculated from the Stejskal-Tanner equation using the gradient sequence in [12] and a b-value of 1000.

Satisfactory tracing results for the first three cases can be found in [9], where a simpler algorithm was used. For the sake of brevity, in this paper we have worked with the most complex case, the *star* (Fig. 2, top left). This image consists of six orthogonal sine half-waves, each of them with an arbitrary radius. Under this scenario the diffusion field experiments variations with the three coordinate axes and there exists a crossing region. Three different tracking results are shown in Fig. 2, each of them for a different seed $V_0 = \{S_1, S_2, S_3\}$. Blue tracts were obtained with an algorithm were parameters were estimated with a NN [11], while green ones correspond to the estimation using the proposed AG.

It can be seen that in both cases the path estimates pass through isotropic zones where different fiber bundles cross. It is also appreciated how both methods differentiate between the totally isotropic zones extrinsic to the tracts and the fiber bundles.

The differentiation between voxels belonging to a fiber or to a very isotropic area, respectively, is attained by mapping the path probabilities given by Eq. (4) into a color scale and classifying them according to some fixed thresholds. Notice that seeds S_1 and S_2 belong to the intrinsic volume (voxels with a very high anisotropy). In this case both methods move through the most probable direction following the main direction of the star in each situation. When extrinsic point S_3 is selected as seed, the algorithms explore in the neighboring voxels until they find a voxel with a high anisotropy value (point P_1). Once P_1 is found, the tracking algorithm proceeds as in the case of S_1 and S_2. Fig. 2 shows how the algorithm finds the proper fiber path whatever (extrinsic or intrinsic) seed voxel is chosen, for both methods of parameters' estimation.

Next, the robustness of the tracking algorithm with both parameter estimation methods is now studied. For the sake of brevity, these experiments were run with parameter s kept constant during the fiber tract estimation (see section 2.5).

The convergence performance for different SNRs is shown in Table 1. The first row in each cell corresponds to tracking results when parameters where estimated using the NN, the second contains the results when the proposed AG is used for this estimation, and the third one shows the values obtained with a slightly modified version of the Bayesian method proposed in [3].

It can be seen that both algorithms (with NN- and AG-based adjustment) converge properly within a wide range of SNRs, with the AG version showing a convergence gain of about 3-6% in all cases. The percentage values for the "cross" and the "earth" test images are very close, while for the "log" case both algorithms exhibit a slightly lower convergence. Comparing our methods with the Bayesian approach, we see that the proposed tracking algorithm performs slightly better when the SNR is low, while the three methods tend to similar results with high SNRs.

Analyzing the simulations of the synthetic images considered, it is seen that convergence results improve whenever the MR image contains branching or crossing areas –as it is the case in real DT-MR images. This is the case of our "cross" image. For this image, the convergence results are improved $\sim 5\%$ when parameter s is modified according to the anisotropy.

4.2 Real images

The proposed tracking algorithm has also been applied to real DT-MR images. Specifically, we have selected the *corpus callosum* of the brain (see Fig. 3).

Simulation results show that whichever parameters tuning-up method is used, the algorithm is able to follow the main fiber bundle directions without getting out of the area of interest. Fig. 3 shows some bundles of properly estimated tracts. Red/green color indicates high/low certainty.

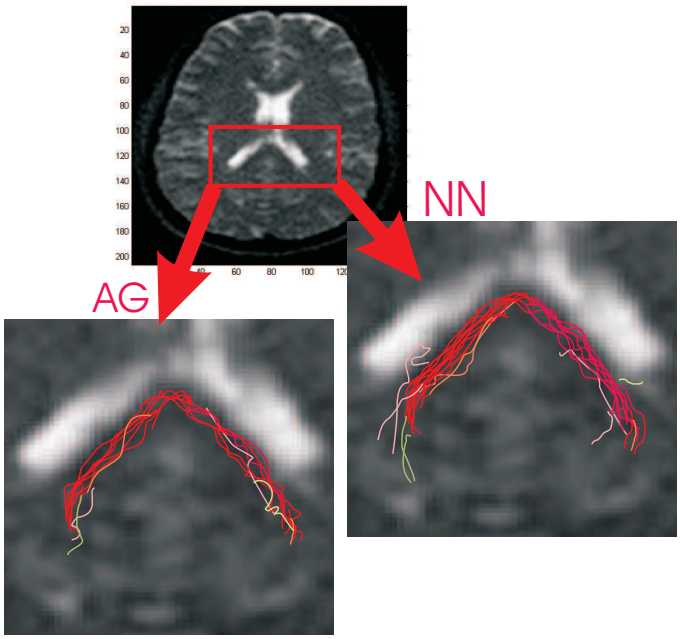

Figure 3: Tracking results for the *corpus callosum* area of the human brain. Left: tracts obtained with the tracking algorithm tuned-up with the proposed AG, Right: parameter estimation with NN.

4.3 Final remarks

The proposed parameter estimation procedure is useful when the volume being varies. For instance, with just 5-10 training iterations (repetitions of the procedure described in 3.1), in synthetic images, or 8-16, in real images, the parameters of the algorithm are fine-tuned so as to get satisfactory results. Note that these previous training times are: (i) always inferior to those required by the NN-based method proposed in [10, 11], (ii) always greatly inferior to the time required to heuristically adjust the parameters, (iii) only required when the scanning conditions vary.

5 Conclusions and Future Work

The work here presented expands upon previous work of the authors on fiber tracking algorithms to be used with DT-MR images. Previous papers presented and improved the basic probabilistic tracking algorithm [9] and

			SNR (dB)					
			5	10	15	20	25	30
Image	Cross	NN	78.3/**82.8**	89.7/**93.6**	92.1/**94.3**	98.3/**98.7**	99.0/**99.0**	100/**100**
		AG	81.2/**85.7**	93.6/**94.5**	94.9/**96.1**	98.8/**98.7**	99.0/**100**	100/**100**
		[3]	76.8	89.0	90.7	97.0	100	100
	Earth	NN	77.7/**76.2**	88.6/**87.5**	89.9/**89.0**	98.2/**98.2**	99.0/**99.0**	100/**100**
		AG	82.1/**79.6**	89.6/**92.5**	93.5/**94.0**	98.8/**98.9**	99.0/**100**	100/**100**
		[3]	74.4	83.2	85.0	97.3	99.2	100
	Log	NN	71.0/**69.7**	82.1/**81.0**	86.1/**85.5**	96.0/**95.8**	98.0/**97.8**	100/**100**
		AG	75.0/**75.2**	85.2/**85.0**	89.9/**87.7**	97.0/**97.2**	98.2/**98.4**	100/**100**
		[3]	68.8	78.3	85.2	96.0	98.0	100

Table 1: Convergence performance for different SNRs values. Cell values represent percentage of right convergence for two configurations of the algorithm: $s = 1/\mathbf{s} = \mathbf{4}$. Each cell shows: top: NN-estimation, middle: AG-estimation, bottom: Bayesian tracking [3].

developed a novel multilayer neural network that helps to tune-up the tracking method [10]. In this paper we have presented an Evolutionary Computation-based algorithm that outperforms the neural network approach.

Numerical simulations have shown that the tracking algorithm that has been tuned-up using the proposed AG-based method is capable of estimating fiber tracts both in synthetic and real images. The robustness and convergence have been studied for different image qualities (SNRs). Results show a convergence gain of about 3-6% with respect to our previous work [10, 11].

The experiments carried out show that an efficient parameter adjustment in conjunction with precise rules to manage and update the pool of future seeds lead to: (i) a better use of computational resources, (ii) a better performance in regions with crossing or branching fibers, and (iii) a minimization of the required human intervention time. The method has been tested with synthetic and real DT-MR images with satisfactory results, showing better computational and convergence properties than already existing Bayesian methods.

6 Acknowledgement

The authors acknowledge the Spanish CICYT for research grant TEC2007-67073/TCM, the Fondo de Investigacin Sanitaria, Spain, for research grant PI04-1483 and the Junta de Castilla y León for grant VA026A07.

References

[1] Bjornemo, M., Brun, A., "White Matter Fiber Tracking Diffusion Tensor MRI," *Master's Thesis*, Linkoping University, 2002.

[2] Ehricke, H.H., Klose, U., Grodd, U., "Visualizing MR Diffusion Tensor Fields by Dynamic Fiber Tracking and Uncertainty Mapping," *Computers & Graphics*, pp. 255–264, 30/06.

[3] Friman, O., Westin, C.-F., "Uncertainty in White Matter Fiber Tractography," *Proceedings of the MICCAI 2005, LNCS 3749*, pp. 107-114, 2005.

[4] Gudbjartsson, H., Patz, S., "The Rician Distribution of Noisy MRI Data," *Magnetic Resonance in Medicine*, pp. 910–914, 34/95.

[5] Kang, N. et al., "White Matter Fiber Tractography Via Anisotropic Diffusion Simulation in the Human Brain," *IEEE Transactions on Medical Imaging*, pp. 1127–1137, 24/05.

[6] Mitchell, M., "An Introduction to Genetic Algorithms", *The MIT Press, Cambridge, MA*, 1996.

[7] Mori, S., van Zijl, P.C.M., "Fiber Tracking: Principles and Strategies – A Technical Review," *Nuclear Magnetic Resonance in Biomedicine*, pp. 468–480, 15/02.

[8] San-José-Revuelta, L.M., "Entropy-Guided Micro-Genetic Algorithm for Multiuser Detection in CDMA Communications," *Signal Processing*, pp. 1572–1587, 85, 2005.

[9] San-José-Revuelta, L.M., Martín-Fernández, M., Alberola-López, C., "A New Proposal for 3D Fiber Tracking in Synthetic Diffusion Tensor Magnetic Resonance Images," *Proceedings of the IEEE Int'l Symp. on Signal Processing and its Applications, ISSPA'07*, Sharjah, United Arab Emirates, 2007.

[10] San-José-Revuelta, L.M., Martín-Fernández, M., Alberola-López, C., "Neural-Network Assisted Fiber Tracking of Synthetic and White Matter DT-MR Images," *Proceedings of the World Congress on Engineering 2007, WEC 2007*, London, United Kingdom, pp. 618–623, 2007.

[11] San-José-Revuelta, L.M., Martín-Fernández, M., Alberola-López, C., "Efficient Tracking of MR Tensor Fields Using a Multilayer Neural Network," *IAENG International Journal of Computer Science*, pp. 129–139, 35/1, 2008.

[12] Westin, C.-F. et al., "Processing and Visualization for Diffusion Tensor MRI," *Medical Image Analysis*, pp. 93–108, 6/02.